Paper published in *Journal of Sound and Vibration* 502 (2021) 116095
https://doi.org/10.1016/j.jsv.2021.116095

A modelling approach for noise transmission through extruded panels in railway vehicles

Hui Li[1], Giacomo Squicciarini[1], David Thompson[1], Jungsoo Ryue[2], Xinbiao Xiao[3], Dan Yao[3], Junlin Chen[3]

[1] Institute of Sound and Vibration Research, University of Southampton, Southampton SO17 1BJ, United Kingdom
[2] School of Naval Architecture and Ocean Engineering, University of Ulsan, Ulsan, South Korea
[3] State Key Laboratory of Traction Power, Southwest Jiaotong University, Chengdu 610031, China

Abstract

The noise inside railway vehicles plays an important role for the comfort of passengers and train crew. In determining the interior noise, the noise transmission through the train floor and sidewalls is particularly important. Modern train body structures are often made of extruded aluminium panels and the current work focuses on modelling the noise radiation from, and transmission through such structures. Use is made of a statistical energy analysis (SEA) approach which is established with the support of a waveguide finite element (2.5D FE) model. The latter is used to study the vibration properties of the extruded panel that are then utilized to calibrate simple equivalent analytical models for the various components of the extrusion. These in turn are used to define the input parameters for the SEA model, e.g. the modal densities and the coupling loss factors between subsystems. With the aid of such a calibration, the predictions from the SEA model of the sound transmission loss and of the radiation efficiency of the extruded panel agree well with measurements and numerical models using the 2.5D FE/BE approach and the VA One software. By following the procedures outlined in this paper, SEA models can be established by using a simple analytical representation of different parts of the extruded panel and hence without the need to develop ad-hoc and computationally expensive numerical models.

Key words: 2.5D FE method, SEA, extruded panel, sound transmission loss, radiation efficiency

1 Introduction

Interior noise in railway vehicles plays an important role in the comfort of the passengers. Train manufacturers dedicate much attention to the development of quieter vehicles, but the prediction of interior noise in trains is still an important problem and poses a significant challenge to researchers and industry alike [1]. Various sources contribute to train interior noise. These include rolling noise, caused by wheel/rail interaction, and aerodynamic noise, caused by flow/structure interaction. The mechanisms of rolling noise [2] and aerodynamic noise generated by train components [3] have been studied to varying degrees and models exist that are capable of predicting their sound power. In order to calculate the resulting sound pressure levels inside a vehicle, reliable models are required for the vibro-acoustic performance of the train floor and wall structures, in terms of both their sound radiation due to a mechanical excitation and the sound transmission through the panels from exterior sources. Many studies exist on the sound transmission and insulation of single/double panels and various different models are available. For instance, Hongisto et al. [4] listed seventeen existing prediction models for double panels and gave a qualitative and quantitative comparison of them. However, to give a good balance between low weight and high stiffness, the structure of a modern train is commonly made of extruded aluminium panels consisting of two outer face plates with intermediate diagonal stiffening strips; thus, none of those models can be used directly. Using traditional finite element (FE) and boundary element (BE) methods poses a significant challenge because of the frequency range of interest (generally up to 5 kHz) and the typical dimensions of a railway vehicle (roughly $3 \times 3 \times 20$ m^3).

Statistical energy analysis (SEA) [5] is often used to study high frequency vibroacoustic problems and it has been used in the prediction of noise transmission through complicated panels. Geissler and Neumann [6], for example, adopted it to study extruded panels, modelling them as sandwich and orthotropic panels. Commercial software, Auto-SEA, was used but not many details were given about the modelling. Later, Brühl et al. [7] applied both a sandwich representation and a more detailed model for their analysis using the Auto-SEA software. Orrenius et al. [8] modelled the acoustic transmission through extruded profiles of railway vehicles by using SEA combined with the 2.5D FE method, including a floating floor assembly. With assistance of SEA, Yao et al. [9] provided a lightweight design approach for a floating floor based on analysis of the vibrational responses of each component of the floating floor structure. In their models, an SEA model of an extruded panel was created in VA One software

based on the periodic structure theory [10], which enables the SEA parameters to be efficiently computed for structural panels with periodic properties. Xie et al. [11] also used the SEA method to predict the vibro-acoustic behaviour of aluminium extrusions. The whole extruded panel was represented by a single subsystem representing global modes and three subsystems representing the local modes of the various strips on the two faces and the interior.

To provide input data for the SEA model, Xie et al. [12] developed an approximate model for the modal densities of plates characterised by different boundary conditions. In addition, the formula for the average radiation efficiency of a lightly damped plate given by Maidanik [13] was slightly modified to give improved estimates for long thin strips [14]. Finnveden [15] used a waveguide (i.e. 2.5D) FE method to estimate modal densities of structures. The waveguide FE models were used to calculate wave propagation characteristics for built-up thin-walled structures, and modal densities of the structures were estimated based on the dispersion relation from these models. Due to the difficulties to derive the coupling loss factors (CLFs), Preis and Borello [16] used a virtual SEA and experimental SEA approach to predict the CLFs in a study of a light rail vehicle. In their experimental SEA the power injection method [17] was utilised in determining CLFs for complex systems. To avoid practical issues for the experimental determination of CLFs, Manguán [18] presented a formulation of reduced SEA models for incomplete systems defined by a set of effective loss factors, which allows some of the model loss factors to be defined that could not be obtained through the power injection method. Sadri et al. [19] introduced a Bayesian method as an alternative way to determine the CLFs to avoid using experimental SEA. Ben Souf et al. [20] evaluated the CLFs based on the wave FE method, taking into account the effect of the different types of uncertainties in coupled structures. Maxit and Guyader [21] presented a dual formulation and a FE model to estimate the CLFs for SEA models. The dual formulation was used to describe the vibration of coupled subsystems and the FE model was employed to calculate the modal information in the case of complex substructures, which allows CLFs to be determined only from the knowledge of the modes of the uncoupled subsystems and the modal damping. Thite and Mace [22] introduced the idea to randomise the properties of a system and average the resulting estimates to achieve robust estimation of CLFs from FE analysis. To determine the power input to the subsystems of the SEA model, Xie et al. [11] divided the power injected to the system into different parts based on the modal densities of the subsystems. Zheng et al. [23] built a structural dynamic model and a computational fluid dynamics model to calculate the excitation on the train body when they investigated noise transmission through extruded train wall structures to the interior.

A common problem with SEA is that it has limitations at low frequencies where the modal density and mode count of the structures are low. Besides, the conventional SEA approach presents some difficulties when it is applied to train floor structures as the typical structures of railway vehicles are rather complex, comprising strips, stiffeners, joints and damping treatments [8]. To overcome these limitations, numerical predictions by means of wavenumber domain finite and boundary element (2.5D FE/BE) coupled methods [24] have been derived to predict the sound radiation efficiency and sound transmission loss of structures that have uniform properties in one direction. A wavenumber domain software, 'WANDS', using this 2.5D approach was previously developed at ISVR, University of Southampton for research purposes [25]. The 2.5D approach only considers the cross-section of the structure by modelling the third direction in terms of a spectrum of wavenumbers, which will greatly reduce the computational time compared with the corresponding 3D numerical models. The 2.5D method has been applied in the literature to study a variety of problems successfully, including composite plates [26], thin-walled beams [27], and rib-stiffened plates [28]. In applications for train floor and walls using the 2.5D method, Kim et al. [29, 30] predicted the radiation efficiency from and sound transmission through part of an actual train floor structure. Zhang et al. [31] provided an extensive parametric study to investigate the effect of different reinforcement rib styles on the sound transmission loss. In Kim et al.'s model [29], the width of the extruded cross-section was 1 m and the total number of degrees of freedom was 1364, including 1012 for FEs and 352 for BEs. To represent the whole train cross-section, a much larger number of elements would be needed. This increases the difficulties in creating the model and increases the computation time significantly as well. In practical applications and at a design stage of a new vehicle, the 2.5D FE/BE approach using bespoke software may be computationally expensive and not offer the flexibility to handle design changes.

Apart from the 2.5D method, the periodic cell method, in which a small finite element model of a periodic cell is used to create an infinite structure, is also an effective way to simulate the vibration and sound transmission loss of large periodic or near periodic structures. Kohrs and Petersson [32] used the periodic cell method to study the structure-borne sound and dispersion characteristics of extruded panels. Yang et al. [33] presented a modelling strategy based on the periodic cell method to predict the sound transmission through honeycomb-cored panels that are periodic in two directions. Orrenius et al. [34] compared the 2.5D FE/BE method and the periodic cell method when determining the sound transmission loss of composite sandwich

structures for interior noise prediction. They showed that the 2.5D method gave better predictions of sound transmission loss below 500 Hz than the periodic cell method while the periodic cell method is more efficient than the 2.5D method.

On the basis of the above background, the aim of this work is to develop an improved SEA model to study the sound radiation efficiency and sound transmission through extruded panels. In this SEA model, several key parameters such as the modal densities of subsystems, radiation efficiencies, and coupling loss factors are derived with assistance of 2.5D FE model calculations. Specifically, a 2.5D FE model is used to define and tune some simple analytical models which are used to obtain the required SEA parameters. Simply supported strips with a reduced width are used to ensure the correct cut-on frequencies. Afterwards, a similar procedure could be used to define the SEA parameters for panels with different geometry which would allow SEA models to be developed for other designs of extruded panels without the need for new and computationally expensive numerical models. In the remainder of the paper, Section 2 presents the 2.5D FE method used to analyse the behaviour of the extruded panel, and Section 3 introduces the SEA model and demonstrates the use of the 2.5D FE method to calibrate some analytical models which are created to obtain the essential parameters required by the SEA model. Section 4 shows how the SEA approach gives predictions for the sound radiation efficiency and sound transmission loss of the extruded panel and compares them with measurements and predictions from the 'WANDS' 2.5D software. The conclusions are given in Section 5.

2 Wavenumber domain analysis for the extruded panel

The cross-section of the extruded panel considered in this work is illustrated in Figure 1. It consists of three bays of equal geometry (see Table 1). The width of the extruded panel is 1 m in the *y* direction; the height is 0.067 m in the *z* direction; where applicable, the length is set to 20 m to represent a typical train vehicle in the *x* direction. The top plate is covered by a layer of rubber and represents the side of the train floor facing into the cabin. The damping loss factors of the top and bottom plates of the panel were measured in experiments by Zhang et al. [31]. In this work, unless otherwise stated an averaged damping loss factor 0.005 is used for the bare aluminium and 0.02 for the top plate which is covered by the layer of rubber [29]. The material properties of the panel are listed in Table 2 [29].

In the remainder of this paper, the term ‘extruded panel’ is used to refer to the whole structure, while ‘strips’ refer to the narrow thin plates that make it up, see for example strips A, B, C in Figure 1. Based on [28], the vibration of the extruded panel can be divided into global and local behaviour. In the global behaviour, the whole structure corresponds to an equivalent homogeneous plate which has the same mass per unit area and bending stiffness as the whole extruded panel. In this case the modes/waves of this equivalent homogeneous plate are defined as ‘global modes/waves’. Conversely, local behaviour corresponds to situations in which the vibration is predominantly confined to one or more strips, resulting in local modes/waves.

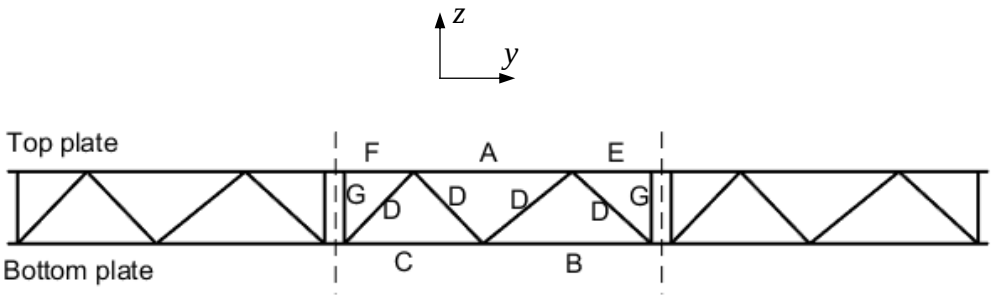

Figure 1. Schematic representation of the extruded panel with identification given to each strip.

Table 1. Geomterical details of the extruded panel.

	Strip A	Strip B	Strip C	Strip D	Strip E	Strip F	Strip G
Width (m)	0.16	0.17	0.14	0.10~0.11	0.08	0.07	0.067
Location	top plate (with rubber)	bottom plate	bottom plate	middle	top plate (with rubber)	top plate (with rubber)	middle

Table 2. Material properties used for the extrusion and the rubber layer [29].

Properties	Young's modulus (E) N/m^2	Poisson's ratio (ν)	Density (ρ) kg/m^3	Thickness (t) mm	Loss factor (η)	Height (H) m
Aluminium	7.0×10^{10}	0.3	2700	2.5	0.005	0.067
Rubber	-	-	1500	4	0.02	-

2.1 2.5D FE model

Wavenumber-based methods are suitable for predicting the vibro-acoustic performance of structures with an invariant cross-section. Here, the 2.5D FE method is adopted; specifically, a

2.5D FE model of this extruded aluminium panel is created in the 'WANDS' software [25]. In the 2.5D FE model, shown in Figure 2, only a two-dimensional cross-section of the structure is meshed in the y-z plane. The extruded panel is composed of two-node plate finite elements and is set to be simply supported at the two side-edges of the bottom plate. The rubber mat attached to the top plate is included in the model by increasing its mass and damping, assuming it has negligible contribution to the bending stiffness. The size of each element is about 10 mm, which is adequate to represent wave modes up to 5 kHz (the model has more than six nodes per bending wavelength along the y direction in each bay for the highest order waves at 5 kHz). The 2.5D FE model in Figure 2 has 348 elements and 1328 degrees of freedom.

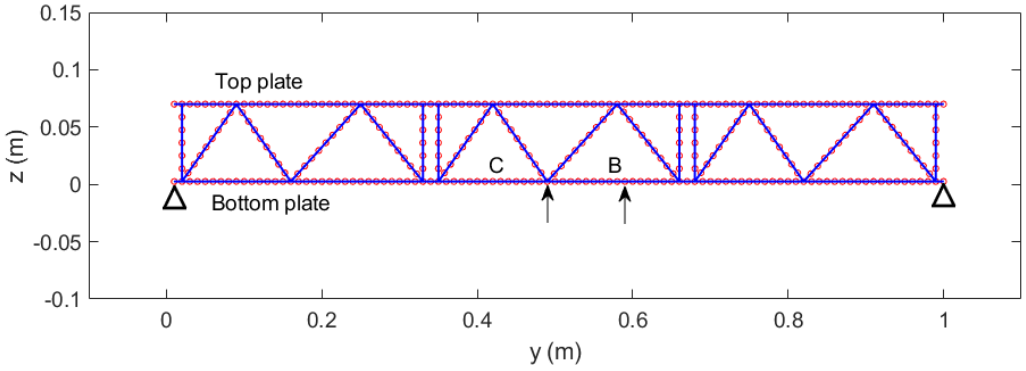

Figure 2. Cross-section model of the extruded panel. Blue lines represent the geometrical shape of the extrusion cross-section, red circles represent the plate finite element nodes in the 2.5D FE model. The two arrows indicate the locations of the mechanical force applied to the structure in Section 4.2.

Harmonic time dependence at circular frequency ω is assumed. The governing equation for plate FE elements is derived in [25] and takes the form

$$\left[\mathbf{K}_4\frac{\partial^4}{\partial x^4}+\mathbf{K}_2\frac{\partial^2}{\partial x^2}+\mathbf{K}_1\frac{\partial}{\partial x}+\mathbf{K}_0-\omega^2\mathbf{M}\right]\mathbf{\Phi}(x)=\mathbf{F}(x) \qquad (1)$$

where $\mathbf{K}_i$ are the stiffness matrices, $\mathbf{M}$ is the mass matrix, $\mathbf{F}(x)$ is a vector of nodal forces, and $\mathbf{\Phi}(x)$ is a vector of nodal displacements. The detailed derivation of these matrices can be found in [25]. If a Fourier transform is applied with respect to x, $\mathbf{\Phi}$ can be expressed in the wavenumber domain as

$$\widetilde{\mathbf{\Phi}}(k_x) = \int_{-\infty}^{\infty} \mathbf{\Phi}(x) \mathrm{e}^{\mathrm{i}k_x x} \mathrm{d}x \tag{2}$$

and, similarly, the force in the wavenumber domain is given by

$$\widetilde{\mathbf{F}}_s(k_x) = \int_{-\infty}^{\infty} \mathbf{F}(x) \mathrm{e}^{\mathrm{i}k_x x} \mathrm{d}x \tag{3}$$

The inverse Fourier transform of Eq. (2) allows the spatial variation to be recovered

$$\mathbf{\Phi}(x) = \frac{1}{2\pi} \int_{-\infty}^{\infty} \widetilde{\mathbf{\Phi}}(k_x) \mathrm{e}^{-\mathrm{i}k_x x} \mathrm{d}k_x \tag{4}$$

Then, Eq. (1) becomes

$$[\mathbf{K}_4(-\mathrm{i}k_x)^4 + \mathbf{K}_2(-\mathrm{i}k_x)^2 + \mathbf{K}_1(-\mathrm{i}k_x) + \mathbf{K}_0 - \omega^2\mathbf{M}]\widetilde{\mathbf{\Phi}} = \widetilde{\mathbf{F}}_s \tag{5}$$

Positive values of wavenumber k_x correspond to waves propagating in the positive *x* direction and vice versa. For the case of free vibration Eq. (5) becomes

$$[\mathbf{K}_s(k_x) - \omega^2\mathbf{M}]\widetilde{\mathbf{\Phi}} = \mathbf{0} \tag{6}$$

with $\mathbf{K}_s(k_x) = \mathbf{K}_4(-\mathrm{i}k_x)^4 + \mathbf{K}_2(-\mathrm{i}k_x)^2 + \mathbf{K}_1(-\mathrm{i}k_x) + \mathbf{K}_0$ the stiffness matrix in the wavenumber domain. To study wave propagation in the extruded panel, the eigenvalue problem in Eq. (6) is solved for ω at given values of real wavenumber k_x. The dispersion relations of waves propagating along the x direction in the undamped panel are shown in Figure 3 with a wavenumber resolution of $\pi/20$. The line corresponding to the acoustic wavenumber is also included in Figure 3 for reference.

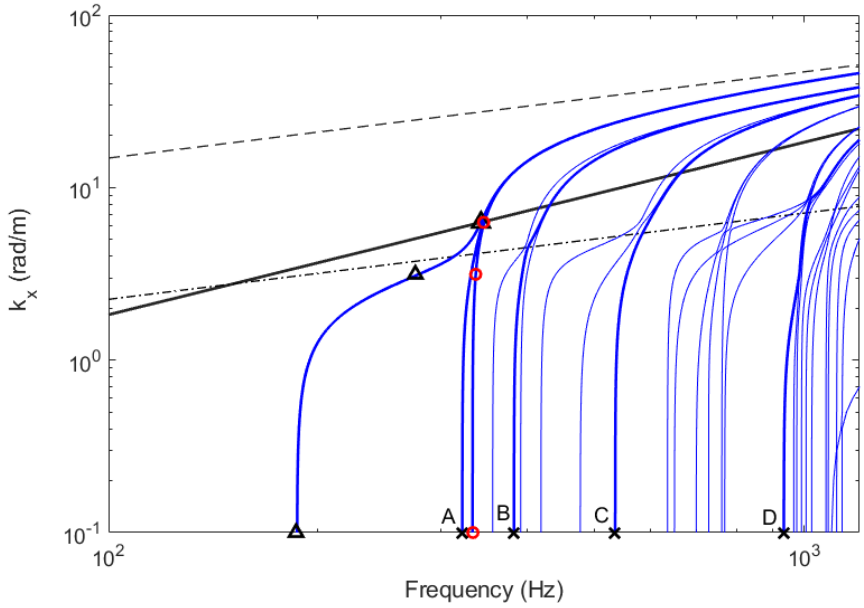

Figure 3. Dispersion curves for the extruded panel. ——: structural wavenumbers; ——: acoustic wavenumber; -·-·-: free bending waves in an infinite plate equivalent to the extruded panel; - - -: free bending waves in an infinite plate equivalent to strips A. The crosses, circles and triangles indicate different wave modes as described in the text.

Some of the trends visible in Figure 3 can be explained in terms of the global and local behaviour. As stated before, in global behaviour the whole structure corresponds to an equivalent homogeneous plate which has the same mass per unit area and bending stiffness as the whole extruded panel. The equivalent bending stiffness can be calculated by [35]

$$B = \sqrt{B_x B_y} \tag{7}$$

where B_x and B_y are the bending stiffnesses along the x and y axis respectively, calculated from the second moment of area per unit length. In this case it is found that $B = 4.77 \times 10^5$ Nm. The average mass per unit area of the extruded panel is 30.93 kg/m^2. Based on reference [36], two asymptotic lines can be calculated to represent the free wavenumber in the equivalent homogeneous plate and in the strips. These are the two broken lines in Figure 3 and are calculated as

$$k = \omega^{\frac{1}{2}}(\mu/B)^{\frac{1}{4}} \tag{8}$$

where μ is the mass per unit area and B is the bending stiffness.

2.2 Mode shapes

In the dispersion diagram, each line represents waves with approximately sinusoidal shapes in the *y* direction, analogous to a thin homogeneous plate strip. The frequencies corresponding to $k_x = 0$ are the cut-on frequencies. Above these frequencies, the axial wavenumber firstly increases rapidly with increasing frequency and then the slope gradually decreases around the first asymptotic line (global behaviour). Having crossed the global behaviour line, the slope increases again before tending asymptotically to the dispersion curves of local waves in the thin strips. This shape of the dispersion curves can be interpreted by considering that the waves change their forms in the extrusion due to the stiffeners. Figure 4 and Figure 5 illustrate the evolution of particular mode shapes as frequency increases. The mode shapes are generated by solving Eq. (5) at a particular frequency ω and at a particular wavenumber k_x corresponding to a point on the dispersion curve in Figure 3. This gives the deformation of the 2D cross-section of the extruded panel. It is then multiplied by $e^{-ik_x x}$ for *x* between 0 and 1 m to obtain the wave modes. In Figures 4 and 5 the real parts of these wave mode shapes are plotted.

Figure 4 represents the shape of the wave corresponding to 'Δ' in Figure 3. The figure is coloured by the displacement in the *z* direction. A global wave, Figure 4(a), becomes local with increasing frequency, Figure 4(b) and (c). Some curves representing local modes do not have this change as they are less affected by the stiffeners. See for instance, the third curve in Figure 3 which represents a purely local wave; its shape is shown in Figure 5 for three different frequencies.

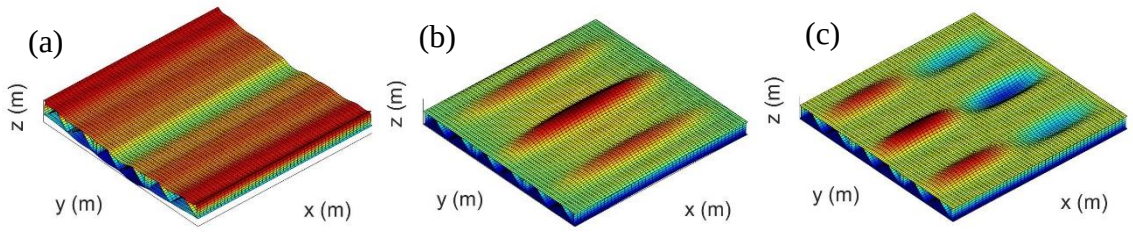

Figure 4. Evolution of the mode shape corresponding to 'Δ' in Figure 3 as frequency increases, the real part of the displacement is plotted, coloured by their *z* coordinates. (a) *f* = 186 Hz, k_x = 0, (b) *f* = 276 Hz, k_x = π, (c) *f* = 343 Hz, k_x= 2π, (k_x, rad/m).

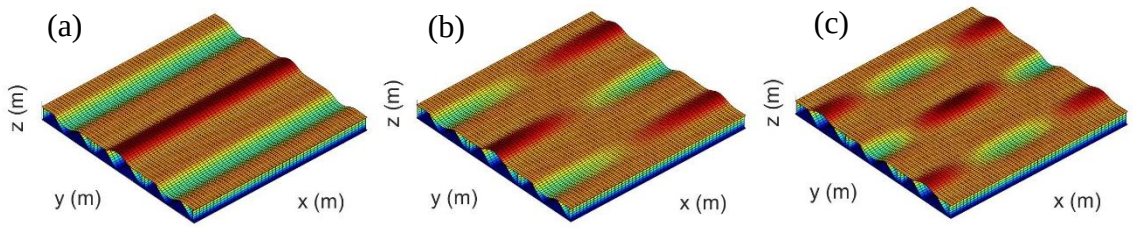

Figure 5. Evolution of the mode shape corresponding to '○' in Figure 3 as frequency increases, the real part of the displacement is plotted, coloured by their *z* coordinates. (a) f = 332 Hz, k_x = 0, (b) f = 337 Hz, k_x= π, (c) f = 346 Hz, k_x= 2π, (k_x, rad/m).

Above the lower dash-dot asymptotic line in Figure 3, local modes are dominant. Orrenius et al. [28] defined this as the 'plate region'. Here, the dispersion curves are clustered in groups with each cluster containing three waves as the extrusion has three identical bays (see Figure 1).

2.3 Cut-on frequencies and modal density

To represent the extruded panel using an SEA model, the modal densities of each subsystem are required. The cut-on frequencies form a lower limit below which no modes are present in a subsystem. By inspecting the wave mode shapes, the cut-on frequencies of strips in groups A, B, C, D (identified in Figure 1) are found and are marked in Figure 3 accordingly. The corresponding mode shapes (at k_x = 0 rad/m) of the four groups of strips are shown in Figure 6(a-d). The vibration of strips A, B and C are clearly seen in Figure 6(a-c). More than one strip of each type vibrates in a given mode due to the repeating nature of the panel geometry. The dominance of strip D is less obvious in Figure 6(d) as various strips are vibrating together. However, when the wavenumber increases (results not reported here), it becomes clearer that this line correponds to waves propagating in strip group D and hence the frequency marked as D is used as the cut-on frequency of the corresponding strip.

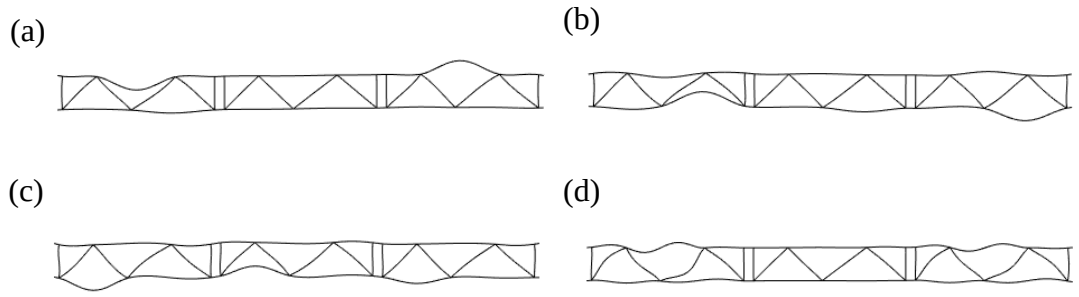

Figure 6. Cut-on mode shapes (k_x = 0 rad/m) of the extruded panel indicated by '✕' in Figure 3. (a) A, (b) B, (c) C, (d) D.

The cut-on frequencies of the strips in groups A, B, C and D are summarised in Table 3. The cut-on frequencies of the other strips (E, F and G) in the extruded panel could not be determined by plotting their deformation. These strips are narrower and their vibration tends to be coupled with other strips nearby.

Table 3. Cut-on frequencies for strips A, B, C and D.

Strips	A	B	C	D
Cut-on frequency (Hz)	332	386	534	934

The dispersion relation analysis of an infinitely long extrusion can also be used to deduce the vibration modes of a structure of finite length L having the same cross-section and with simply supported boundary conditions at the ends. When half the wavelength, or a multiple of it, is equal to L, the corresponding frequency is one of the natural frequencies of the finite structure. In the case of the train floor, L is assumed to be 20 m. Therefore, at the natural frequencies of a 20 m extruded panel, the wavenumbers in the x direction are

$$k_x = \frac{n\pi}{L}, \text{ for } n = 1, 2, 3, \ldots \quad (9)$$

Following this procedure, each point in Figure 7(a) represents an estimate of the natural frequency of the 20 m long train floor. From this, the overall modal density of the extruded panel can be determined from the number of modes in each 1/3 octave frequency band as

$$n(f) = \frac{\text{Number of modes}}{f_2 - f_1} \tag{10}$$

where f_1 and f_2 are the lower and upper limits of each 1/3 octave frequency band. The modal density derived from this is shown in Figure 7(b). The sudden increase in the modal density between 250 and 400 Hz is due to the cut-on of local modes above the frequencies listed in Table 3.

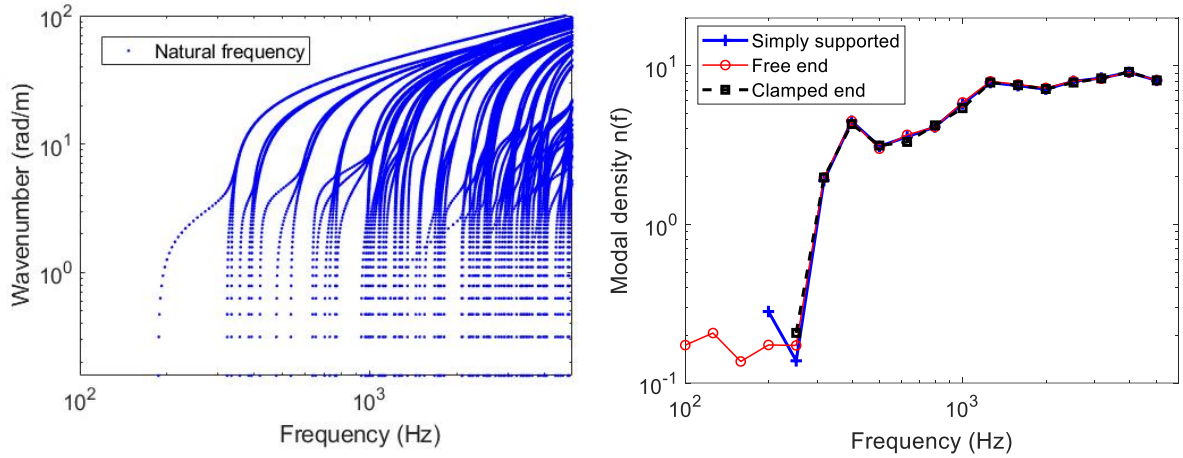

(a) (b)

Figure 7. (a) Natural frequencies of a 20 m long train floor obtained from the dispersion curve, simply supported at the two ends, (b) modal density calculated by the 2.5D FE model.

The results found in this section for the cut-on frequencies and the modal density of the extruded panel have been determined under the assumption of simply supported boundary conditions at the sides and at the ends of the floor. Estimates of the modal densities of the extruded panel under free/clamped boundary condition at the ends are also plotted in Figure 7(b) but they only have noticeable difference at low frequency.

3 SEA approach for modelling extruded panels

In this section an SEA model similar to the one presented by Xie et al. in [11] is applied to the extruded panel. The vibration properties analysed in Section 2 are adopted to determine and calibrate equivalent analytical models that can give the modal densities and the radiation efficiencies of the subsystems that represent various parts of the extruded panel.

3.1 Principle of the SEA method

The general energy balance equation in an SEA model is written as [37]

$$P_{\text{in},i} = P_{d,i} + \sum_{i \neq j} P_{i,j} - \sum_{i \neq j} P_{j,i} \tag{11}$$

where $P_{\text{in},i}$ is the power input to the i^{th} subsystem, $P_{d,i}$ is the dissipated power, $P_{i,j}$ is the power flowing from subsystem i to subsystem j, and $P_{j,i}$ is the power flowing back from subsystem j to subsystem i.

To apply the SEA method to this extruded panel, subsystems need to be defined. Based on the modal analysis in Section 2.1 and 2.2, below the cut-on frequency of the modes in the local strips, only global modes exist in the extruded panel. When the local modes in the strips are excited, the local modes will dominate the vibration as well as the radiation but modes reflecting global behaviour are still present, as seen in the dispersion curves. It is therefore appropriate to separate the vibration of the extruded panel into the global and local modes subsystems in the SEA model. The plates on the two sides will radiate sound directly to the surrounding environment while the middle stiffeners will not. Moreover, the middle stiffeners introduce a vibration level difference between the two outer faces which would not be found if the strips were all part of a single SEA subsystem, e.g. an equivalent plate. Therefore, the two face plates and the middle stiffeners are separated in different local subsystems. The division into four subsystems preserves these features but is much more efficient than a subdivision based on all the individual strips.

The modes of the extruded panel often contain motion of more than one strip. This behaviour is strongest within the strips on the face plates, which will be considered as modal interaction within each subsystem. The coupling between the face strips and middle stiffeners will be considered as energy transmission from one subsystem to another, through their coupling loss factors.

Figure 8 shows a schematic representation of the six-subsystem SEA model created by Xie et al. [11] to predict the vibroacoustic behaviour of aluminium extrusions. Four subsystems were used to model the extruded panel: three of these are for the local behaviour (top plate, bottom

plate and middle stiffeners), and one is for the global modes. Two additional subsystems were used to model the acoustic cavities on either side. The couplings between the subsystems are indicated by the arrows.

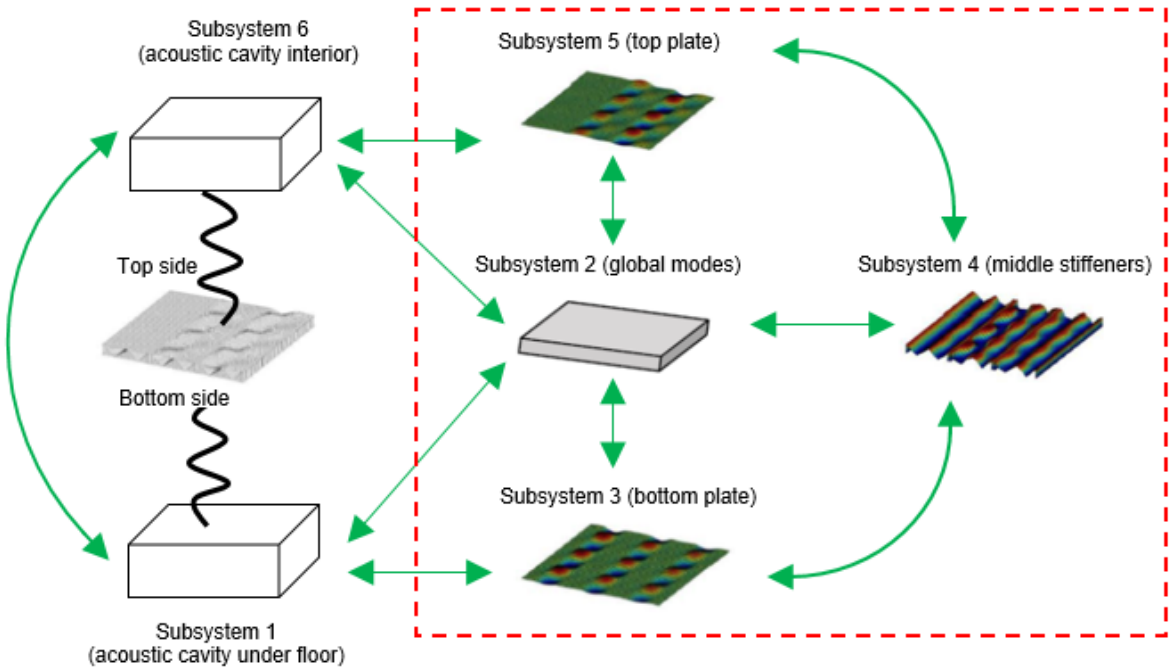

Figure 8. The subsystems used to model the extrusion and the SEA model, redrawn from [11]. The extruded panel is represented by the four subsystems in the red dashed box. Arrows indicate couplings between subsystems.

Assuming that there is no direct coupling between the local modes on the two sides of the extruded panel, there are five different types of coupling in this SEA model; they are

1. Non-resonant sound transmission [37] between the two cavities through the extruded panel: subsystem (1) to subsystem (6).
2. Coupling between cavities and global modes: (1) to (2) and (2) to (6).
3. Coupling between cavities and local modes: (1) to (3), and (5) to (6)
4. Coupling between global modes and local modes within the panel: (2) to (3), (2) to (4), (2) to (5).
5. Coupling between local modes within the panel: (3) to (4), (4) to (5).

In this paper, the six-subsystem framework of the current SEA model is based on Xie et al. [11] but some changes are made based on the modal analysis in Section 2.1 and 2.2. In Xie et al.'s

SEA model [11], the modal densities of each subsystem were estimated as asymptotic values based on plate theory, which failed to predict the cut-on frequencies of the local subsystems correctly. In the current SEA model, a simple analytical model will be employed to predict the modal densities of each subsystem with the aid of the 2.5D approach. Besides, an equivalent width will be used for the strips to account for the effect from the boundary whereas Xie et al. simply considered the strips in the extruded panel as simply supported. Third, the coupling loss factors between local subsystems are based on the relatively accurately predicted modal densities in this work, instead of using the asymptotic modal densities for a thin plate used by Xie et al. [11] which are less accurate for the strips in the extruded panel. Furthermore, the method to calculate the power input to the global and local subsystems was not elaborated in Xie et al.'s work but it is discussed for this current SEA model.

Kim et al. [29, 30] studied the sound transmission loss of an extruded panel with and without the air cavity between plates and found that acoustic coupling between the plates is not significant. The air cavity between the plates is therefore omitted as the structural connections are more important for this structure [31].

For the simulation of sound transmission, power is injected into one of the acoustic cavities and the power transmitted to the other one is determined. For this, both the resonant and non-resonant transmission need to be considered. The resonant transmission is included in the SEA model by the coupling through the panel's subsystems. The non-resonant sound transmission between two cavities depends mainly on the mass per unit area and is modelled by the 'mass law' through the coupling between subsystems (1) and (6) [37]. For the simulation of sound radiation, power is injected into one or more structural subsystems and the power radiated into the acoustic cavities is determined.

3.2 Modal densities of the subsystems

In order to propose a simplified approach that ultimately does not require a 2.5D FE model, it is useful to predict the SEA inputs making use only of geometrical and material properties. For the local modes, equivalent strips could be used with an appropriate choice of boundary conditions at the sides. However, the lateral boundary conditions of strips assembled in an extruded panel cannot be defined exactly. It is expected that they would correspond to a condition between simply supported and clamped [37]. The first natural frequencies obtained

analytically with different boundary conditions [35] for various strips in the 20 m long train floor are listed in Table 4 and are compared with the 2.5D FE results from Section 2. These results indicate that the 2.5D results lie between the CSSS and CSCS results.

Table 4. Cut-on frequency of local modes of the extrusion.

Note*	Boundary condition	strip group A	strip group B	strip group C	strip group D
(1)	SSSS	175 Hz	213 Hz	314 Hz	508 Hz
(2)	CSSS	274 Hz	332 Hz	490 Hz	793 Hz
(3)	CSCS	397 Hz	482 Hz	711 Hz	1152 Hz
(4)	2.5D FE calculation	322 Hz	386 Hz	534 Hz	934 Hz

* (1) the strips are assumed to be simply supported on the four edges (SSSS), (2) clamped on one their longer edges and simply supported on all others (CSSS), (3) they are clamped on their two longer edges, setting the shorter edges simply supported (CSCS), and (4) FE calculations are read from the curves A, B, C, D in Figure 3.

An alternative approach is to adjust the width of each strip. The boundary conditions are assumed to be simply supported at all edges and an equivalent width for each strip is determined so that their first natural frequencies correspond to the values provided by the 2.5D FE calculations. This is achieved by applying a modified width b' in the equation:

$$f_{m,n} = \frac{\pi}{2}\left[\left(\frac{m}{a}\right)^2 + \left(\frac{n}{b'}\right)^2\right]\sqrt{\frac{B}{\mu}} \quad m,n = 1,2,3\cdots \tag{12}$$

where a is the strip length, μ is the material mass per unit area and B is the bending stiffness. For example, strips A are of width $b = 0.16$ m, and their cut-on frequency, obtained from the 2.5D FE calculation, is 322 Hz. A modified width $b' = 0.12$ m gives the required cut-on frequency. The other modified widths are summarised in Table 5 and correspond to 74%-77% of the full width of the strips. Strips E, F and G that could not be identified clearly in the dispersion plot are assigned a width ratio of 0.75.

Table 5. The equivalent width of each strip.

Length	Group A	Group B	Group C	Group D	Group E	Group F	Group G
Original	0.16 m	0.17 m	0.14 m	0.11 m	0.08	0.07	0.0675 m
Equivalent	0.12 m	0.1275 m	0.108 m	0.081 m	0.06 m	0.053 m	0.051 m
Ratio	0.75	0.75	0.77	0.74	0.75	0.75	0.75

To simplify the procedure further, the same factor can be adopted for all the strips and this is chosen to be 0.75. The modal densities of the local subsystems (subsystems 3-5) can then be calculated from Eq. (10).

The modal density of the global mode subsystem (subsystem 2) is found based on the plate model equivalent to the whole extruded panel. The total modal density is the sum of the modal densities of the global and local subsystems and is compared in Figure 9 with the results from the 2.5D FE model. The modal density calculated using the analytical models is generally in good agreement with the results from the 2.5D calculation, although at high frequency it is underestimated by about 20%.

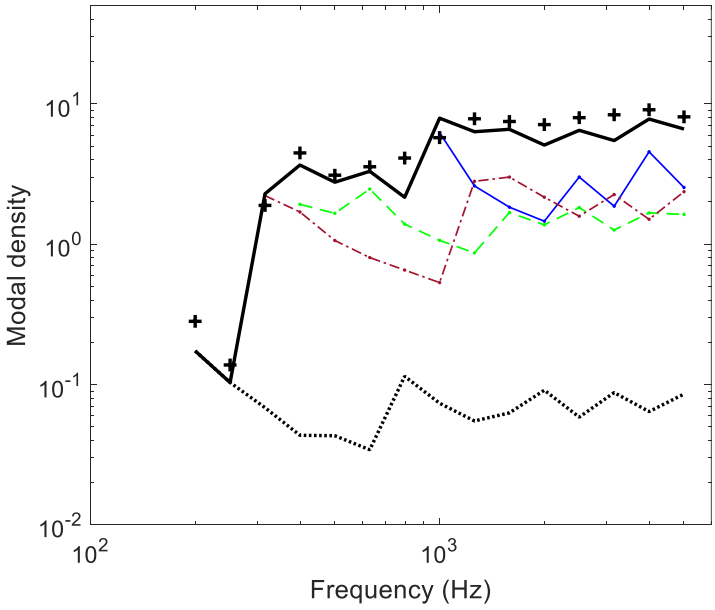

Figure 9. Modal density of the 20 m long train floor. - - -: the modal densities of local subsystem 3, ——: the modal densities of local subsystem 4, -·-·-: the modal densities of local subsystem 5, ·····: the modal densities of global subsystem 2, ——: total modal density. +: 2.5D FE calculation.

The proposed idea to adjust the width of the strips provides satisfactory estimates of the modal densities of each subsystem of the extruded panel, although some differences remain. The underestimate of the modal density at higher frequency occurs because the modified width of the strips cannot fit equally well the higher order cut-on frequencies. A frequency-dependent equivalent width of the strips could be used but it is difficult to determine the higher order cut-on frequencies from Figure 3 as the strips tend to vibrate together at high frequency.

3.3 Determining coupling loss factors

3.3.1 The non-resonant coupling

The direct coupling between the source room and the receiving room (subsystems (1) and (6)) represents the non-resonant transmission path. This path is only expected to be significant below the critical frequency of the global motion of the extruded panel, which occurs at 151 Hz. Moreover, there are no modes in the panel until the cut-on of global modes at 186 Hz, so non-resonant transmission can be expected to be dominant up to that frequency. In this work, the non-resonant transmission is considered in the SEA model for all frequencies and it is only included in the sound transmission loss calculation. The non-resonant coupling in the SEA model is modelled by using the appropriate coupling loss factor between two cavities through a plate

$$\eta_{16} = \frac{c_0 S}{4\omega V_s}\tau, \quad \eta_{61} = \frac{c_0 S}{4\omega V_r}\tau \tag{13}$$

where η_{16} is the CLF from the source room to the receiving room and η_{61} is the other way around, c_0 is the speed of sound in air, S is the area of the plate, V_s is the volume of the source room, V_r is that of the receiving room, and τ is the transmission coefficient from the source room to the receiving room, or vice versa. Specifically, τ is estimated from $R = 10\log_{10}(1/\tau)$, where R is the sound transmission loss through a homogeneous plate with the same mass per unit area as the extruded panel, based on the 'mass law' [38] under diffuse incidence:

$$R \approx 20\log_{10}\left(\frac{\omega\mu}{2\rho_0 c_0}\right) - 5 \tag{14}$$

where μ is average mass per unit area of the extruded panel, 30.93 kg/m^2.

3.3.2 Coupling between global/local modes and acoustic cavity

The CLFs from plates to an acoustic cavity can be modelled in terms of the radiation efficiency of the structure [37]. Therefore, the CLFs between the subsystems representing global and local modes (subsystems 2, 3, and 5) and those representing the acoustic cavities (subsystems 1 and 6) with which they are in direct contact are expressed as

$$\eta_{gc,}\eta_{lc,} = \frac{\rho_0 c_0 \sigma}{\omega \mu} \tag{15}$$

where μ is the mass per unit area, 30.93 kg/m^2 for global modes subsystem, 6.86 kg/m^2 for the subsystems related to the bottom plate and 12.86 kg/m^2 for the top plate with rubber cover. σ in Eq. (15) is the radiation efficiency. For the global modes, the radiation efficiency is obtained by using a modal summation approach and averaging the results over multiple forcing points [39] for the equivalent panel introduced in Section 2.1. As the extruded panel represents a part of the train floor structure, it is assumed it is baffled when calculating the radiation efficiency of the global modes as well as the local modes. The same radiation efficiencies are used for both the sound transmission loss and sound radiation investigation in this work. The first six modes in the width direction and 150 modes in the length direction (900 modes in total, covering most of the modes below 5 kHz) were used for the modal summation. The result is calculated in narrow frequency steps and converted to 1/3 octave bands, giving the results shown in Figure 10. Because the critical frequency of the whole structure is low [14], the radiation efficiency of the global modes tends to unity above 150 Hz. The radiation efficiency of the global modes is also predicted by using the 2.5D FE/BE method (WANDS software) [25] based on the equivalent panel model and it is compared with the value obtained from the modal summation approach in Figure 10. They show very close agreement.

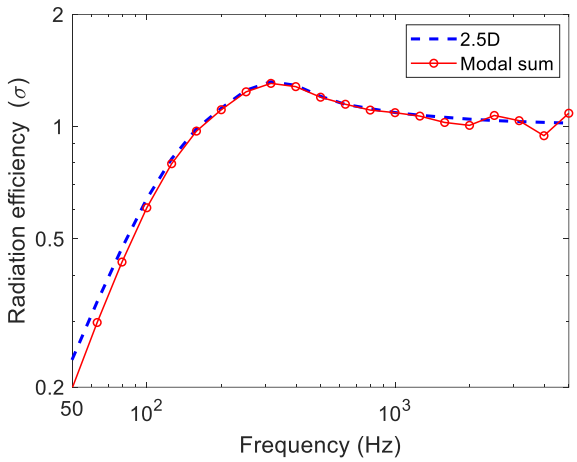

Figure 10. Radiation efficiencies of the global modes obtained by using modal summation approach and by the 2.5D FE/BE approach, results are calculated based on the equivalent panel that represents the whole structure.

For local mode subsystems, all the strips involved can make contribution to the overall radiation efficiency. Figure 11 shows the radiation efficiencies of strips on the two sides of the extruded panel obtained by using the modal summation approach and assuming simply supported boundary conditions. The equivalent widths of the strips derived in Section 3.2 are used and their lengths is set to 20 m. The first six modes in the width direction and 600 modes in the length direction (3600 modes in total, covering most of the modes below 5 kHz) were chosen to calculate the radiation efficiencies of the strips. From Figure 11 it can be seen that the radiation efficiencies drop sharply above the fundamental natural frequencies of the strips once the axial wavenumber k_x exceeds the acoustic wavenumber. They rise to another peak above the cut-on frequency of the second mode. Between the fundamental natural frequency and critical frequency of the strips, acoustic short-circuiting occurs, leading to these large drops in the mid frequency region [38]. At high frequency the radiation efficiencies tend to unity. To verify the predicted radiation efficiencies of the strips, the 2.5D approach was used to calculate their radiation efficiencies and they are compared with the result of the modal summation approach in Figure 11. The comparison is satisfactory and indicates that the number of modes is sufficient to calculate the radiation efficiencies of the strips.

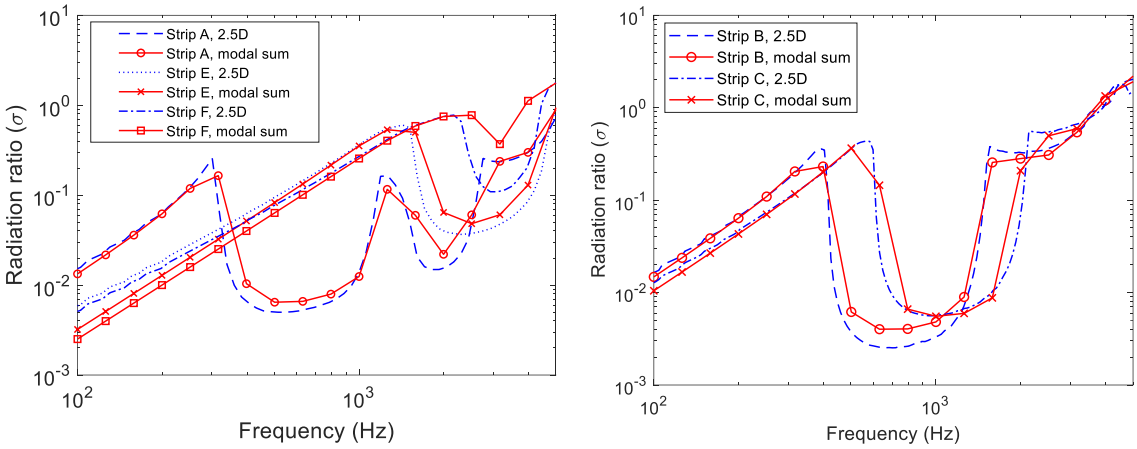

(a) (b)

Figure 11. Radiation efficiencies of the strips obtained by the modal summation approach and by the 2.5D approach. (a) strips on the top plate, (b) strips on the bottom plate. The strips' names are identified in Figure 1.

In the SEA model, the radiation efficiency of the local subsystems is calculated as the area-weighted average of the radiation efficiencies of the strips included in the subsystem. This is based on the assumption that the radiated total power from the local mode subsystem on each side is the sum of the contributions from each of its strips, neglecting any cross coupling effects. It is also assumed that the average vibration of each strip is equal [11]. The average of the radiation efficiency is expressed as

$$\overline{\sigma} = \frac{1}{S}\sum_{i} S_i \sigma_i \tag{16}$$

where σ_i is the radiation efficiency of each strip, S_i is the area of each strip and S is the total surface area in each subsystem. Once the radiation efficiencies of global and local modes have been determined, the CLFs from the extruded panel subsystems to the cavities can be calculated with Eq. (14). The CLFs from the cavities to the global and local modes can be obtained based on the consistency relationship [37].

$$n_i \eta_{ij} = n_j \eta_{ji} \tag{17}$$

3.3.3 Coupling between global and local modes

There is little relevant research on the CLFs between global and local modes of a panel apart from Xie et al. [14]. A related problem is associated with the wave propagation in beam-plate systems [40, 41], in which the beams will generate long wavelength waves. When the long wavelength waves propagate along the stiff beams they will transmit power to the attached plates which will generate short waves in these attached plates. If the difference in terms of their wavelength is large, the plates will mainly introduce damping and represent a locally reacting impedance to the beam behaviour. The wavelengths of the local waves in the strips are around one fifth of that of the global waves in the extrusion, which is reflected by the two asymptotic lines in Figure 3. The extrusion can therefore be considered to be analogous to a beam-plate system, with the global modes equivalent to the beam and the local modes to the strips. An expression for the CLFs from global modes to local modes was therefore given by Xie et al. [11] as

$$\eta_{gl} \approx \frac{\mu_l p}{\mu_g k_l D} \tag{18}$$

where μ_l is the mass per unit area for the local modes and μ_g is the mass per unit area for the global modes, k_l is the wavenumber in the strips, D is the width of the whole extrusion, and p is the number of strips so that p/D means the number of strips per unit width of the plate. The CLFs from the local to the global subsystems can be obtained from the consistency relationship in Eq. (17).

3.3.4 Coupling between local mode subsystems

The couplings between local mode subsystems include couplings between subsystems (3) and (4), and between subsystems (4) and (5). The types of joints in Figure 1 can be divided into groups, illustrated in Figure 12. According to Craik [37], the angle between the strips does not affect the transmission coefficient very much, thus joint types (a) and (b) in Figure 12 are equivalent. The joints that connect strips G and E and that connect G and F are considered as corner joints, Figure 12(c), as the strips at the ends of this unit are very short.

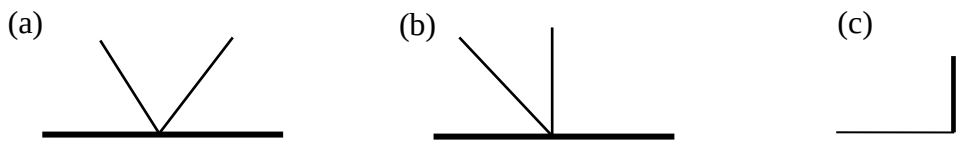

Figure 12. Joints used in the extruded panel, (a) symmetrical cross joint, (b) non-symmetrical cross joint, (c) corner joint.

Approximate expressions to predict the transmission coefficients through such joints are provided by Craik [37]. The bottom plate and the middle stiffeners are of the same material and thickness. The transmission coefficient of the cross joints connecting them is calculated as 0.084. The top plate has an added layer of rubber, which increases its mass. The transmission coefficient through a cross joint from the middle stiffeners to the top plate is 0.084 and in the reverse direction is 0.074. The transmission coefficient through a corner joint from the middle stiffeners to the top plate is calculated at 0.351 and in the reverse direction is 0.300. Once the transmission coefficients between strips are determined, the CLF between two strips is calculated by using [37]

$$\eta_{ij} = \frac{Lk_i\tau_{ij}}{\pi\omega n_i(f)} \tag{19}$$

where τ_{ij} is the transmission coefficient through a cross joint or a corner joint. Then the CLFs between different local mode subsystems can be derived by combining these individual CLFs. The power flow from the local modes on the source room side, *s*, to the local modes of the intermediate strips, *i*, consists of the contributions of all the strips on the source room side (the influence from the ends of this unit is ignored). Therefore,

$$W_{si} = \omega m_B \left\langle \overline{v_B^2} \right\rangle \eta_{BG} + 3\omega m_B \left\langle \overline{v_B^2} \right\rangle \eta_{BD} + 3\omega m_C \left\langle \overline{v_C^2} \right\rangle \eta_{CD} + \omega m_C \left\langle \overline{v_C^2} \right\rangle \eta_{CG} \tag{20}$$

where W_{si} is the power transmitted from the source room side to the intermediate strips, m_i is the mass of the strip and $\left\langle \overline{v_i^2} \right\rangle$ is its mean-square velocity, η_{ij} is the CLF from strip *i* to strip *j*. The subscripts B, C, D and G refer to the corresponding groups of strips. The mean-square velocity of the strips may vary because the excitation may be localised to a particular position. However, to derive a more general CLF from the strips on the source room side to the

intermediate strip, it can be assumed that the strips in each subsystem have the same mean square velocity, which yields

$$W_{si} = \omega m_s \left\langle \overline{v_s^2} \right\rangle \eta_{si} \tag{21}$$

where m_s is the total mass of the strips on the source room side, $\left\langle \overline{v_s^2} \right\rangle$ is the mean square velocity of the plate strips on the source room side, η_{si} is the CLF from subsystem s to subsystem i. Thus, by assuming each strip has similar mean square velocity [14], the CLF between local modes from the source room side to the intermediate stiffeners is

$$\begin{aligned} \eta_{si} &= \frac{m_B\eta_{BG} + 3m_B\eta_{BD} + 3m_C\eta_{CD} + m_C\eta_{CG}}{m_s} \\ &= \frac{4\frac{Lk_s\tau_{\text{cross}}}{\pi\omega}\left(\frac{l_B}{n_B(f)} + \frac{l_C}{n_C(f)}\right)}{l_B + l_C} \end{aligned} \tag{22}$$

where k_s is the wavenumber of the strips on the source room side, L is the length of joint, l is the width of the strips and τ_{cross} is the transmission coefficient given by Craik [37]. Similarly, the power transmitted from the intermediate strips to the receiving room side can be derived. The corresponding CLF can be calculated by

$$\begin{aligned} \eta_{ir} &= \frac{m_G\eta_{GE} + 2m_D\eta_{DE} + 4m_D\eta_{DA} + 2m_D\eta_{DF} + m_G\eta_{GF}}{m_i} \\ &= \frac{2\frac{Lk_i\tau_{\text{corner}}}{\pi\omega}\left(\frac{l_G}{n_G(f)}\right) + 8\frac{Lk_i\tau_{\text{cross}}}{\pi\omega}\left(\frac{l_D}{n_D(f)}\right)}{2l_G + 4l_D} \end{aligned} \tag{23}$$

where k_i is the wavenumber of the intermediate strips and τ_{corner} is again the transmission coefficient given by Craik [37]. In the reverse direction, the CLFs between local modes can be obtained by using the consistency relationship in Eq. (17).

4 Prediction of the SEA model

The SEA model, together with the parameters derived above, is used to predict the sound transmission loss of the extruded panel discussed in this paper, as well as its sound radiation efficiency. The SEA model is arranged to represent two reverberant chambers connected by

the extruded panel. The volumes and loss factors of the source and receiving room are arbitrary and do not affect the sound transmission loss or radiation efficiency, but they are chosen here to replicate the reverberant chambers used in previous measurements [42]. The volume of the source room is $126\ \mathrm{m}^3$ and is located on the side of the bottom plate of the extruded plate (Figure 1) and the volume of the receiving room is $348\ \mathrm{m}^3$. The extruded panel area is set as $20\ \mathrm{m}^2$. The loss factors of the two chambers are calculated from measured reverberation times (T_R) [42] by using $\eta_{1(6)} = 2.2/(fT_R)$. For the extruded panel, Xie et al. [11] gave the experimental result of the damping loss factor of the global modes as $\eta_2 \approx 0.045$ for all frequencies.

Where comparisons are given with the 2.5D approach (for the radiation efficiency on either side), for consistency, local subsystems 3 and 4 are assigned a damping factor of 0.005 and local subsystem 5 (the bottom plate, which is covered in rubber) has a damping loss factor of 0.02 at all frequencies. However, in subsequent results, where comparisons are made with the measured results of the sound transmission loss and radiation efficiency, the local subsystems are assigned measured frequency-dependent values of damping loss factors [30, 31].

4.1 Sound transmission loss

To simulate the sound transmission loss of the extruded panel, sound power is given to the source room, and the SEA model is used to predict the sound pressure in the receiving room. The response of the panel under acoustical excitation in a transmission suite is predicted by the SEA model and they are compared with experimental data from [11] and previous results predicted by Xie et al. [11]. In this section, for consistency with the measurements, the measured values of the damping loss factor [30, 31] are used in the current SEA model for the local subsystems, although it is found that this only has a small effect on predicted results compared with the constant values used above.

To make a direct comparison of the vibrational levels on the two sides of the panel, the power input into the source room in the SEA model is adjusted according to the measurements to make the sound pressure level in the source room the same as the measured values. The vibrational response of the panel to the acoustic excitation is shown in Figure 13. The current SEA model does not give predictions below the 200 Hz band because below the cut-on frequency of the global modes, 186 Hz, the input power does not excite the four subsystems

that represent the extruded panel. Instead, it is all transmitted from the source room to the receiving room directly through the non-resonant path. Xie et al. used an approximate asymptotic expression for the modal density of the global modes [11], which gave nearly constant values over the whole frequency range, which explains that their prediction could give predictions at low frequencies.

From Figure 13, Xie et al.'s SEA model gave good predictions of the vibrational response on the excitation side but underestimated it on the receiving side. The current SEA model slightly underestimates the response on the excitation side but captures the trend and average values of the response on the receiving side, although large errors appear in the 400 Hz and 1250 Hz bands. The fluctuation appearing in the vibrational levels on the two sides of the extruded panel predicted by the current SEA model is a reflection of their modal densities, which were shown in Figure 9. For the vibration level difference, the current SEA model shows large differences with the measurement between 315 and 630 Hz but good agreement above 800 Hz. Xie et al.'s SEA model did not agree with the measurement at high frequency but was closer to the measurement at low frequency. However, below the cut-on frequency of the global modes, only the non-resonant path exists in an SEA sense, and predictions for the panel obtained from an SEA model in that frequency range violate the SEA assumptions.

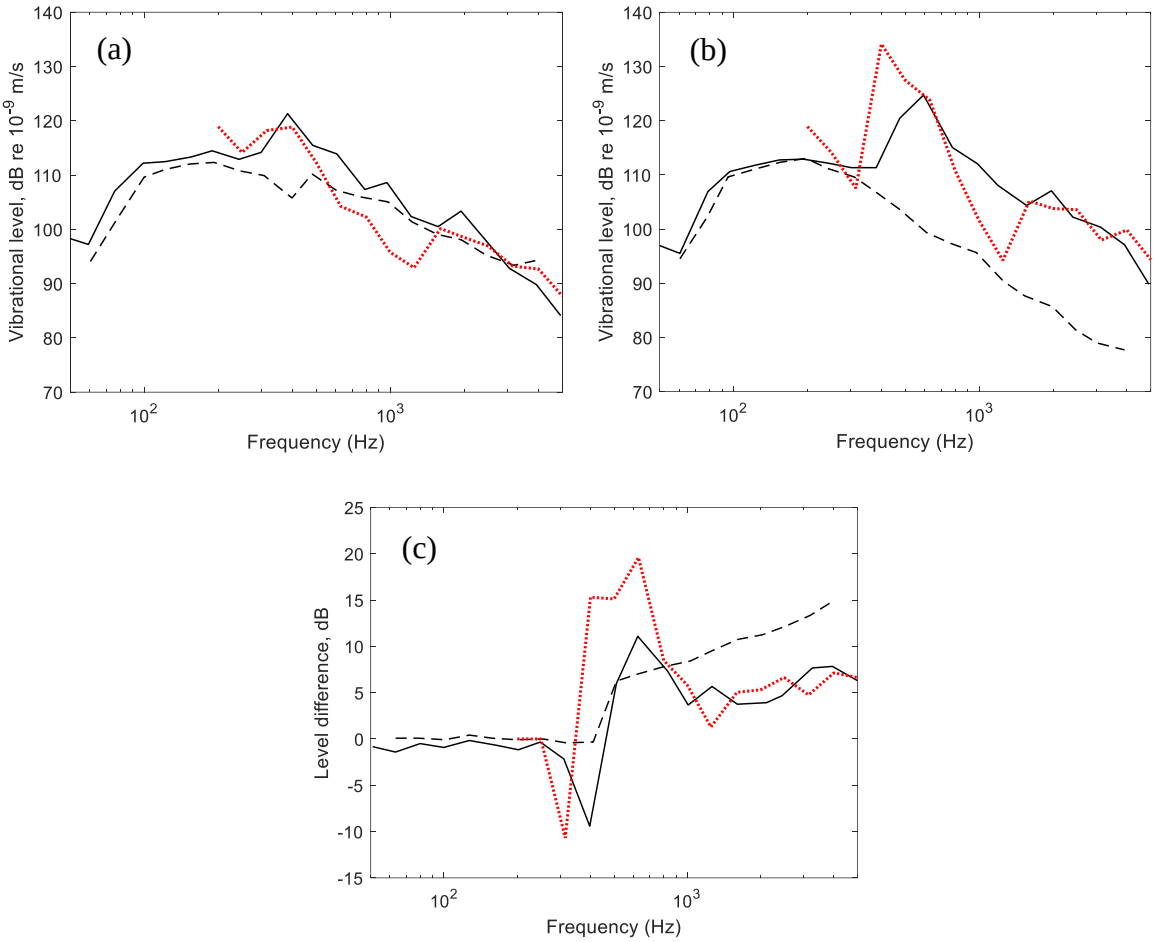

Figure 13. (a) Predicted and measured vibration level on the excitation side for acoustical excitation, (b) vibration level on receiving side, (c) vibration level difference between the two sides of the extruded panel. ——: experimental [11]; – – –: Xie et al.'s SEA [11]; ·····: current SEA.

The sound transmission loss is obtained from the difference between the sound pressure levels in the two rooms. The mean square sound pressure in the source and receiving rooms can be calculated by $\langle \overline{p_1{}^2} \rangle = \rho c_0^2 E_1/V_1$ and $\langle \overline{p_6{}^2} \rangle = \rho c_0^2 E_6/V_6$, where E_1, E_6 are the energies in the source and receiving rooms and V_1, V_6 are their volumes. The sound transmission loss is calculated by [38]

$$R = L_{p1} - L_{p6} + 10\log_{10}\left(\frac{S}{A_6}\right) \tag{24}$$

where L_{p1} is the sound pressure level in the source room, L_{p6} is the value in the receiving room, S is the surface area of the panel, and A_6 is the total absorption area in the receiving room,

expressed as $A_6 = 55.26V_6/(c_0T_{60,r})$, with $T_{60,r}$ the reverberation time. The sound transmission loss of the extruded panel calculated by using the current SEA model is given in Figure 14. It is compared with the result obtained by Xie et al.'s SEA model [11] and with the measured data from references [24, 42]. Xie et al.'s SEA model and the current model do not have significant differences below 1000 Hz. However, above 1000 Hz, the sound transmission loss obtained by the current SEA model shows better agreement with the measurement. The value of R_w according to ISO 717–1 [43] obtained from the current SEA model is 34 dB, close to the measured ones (34 dB and 31 dB) while the prediction from Xie et al.'s SEA model is 36 dB, about 3 dB higher than the measured values. This is a consequence of the improved estimate of the vibration levels.

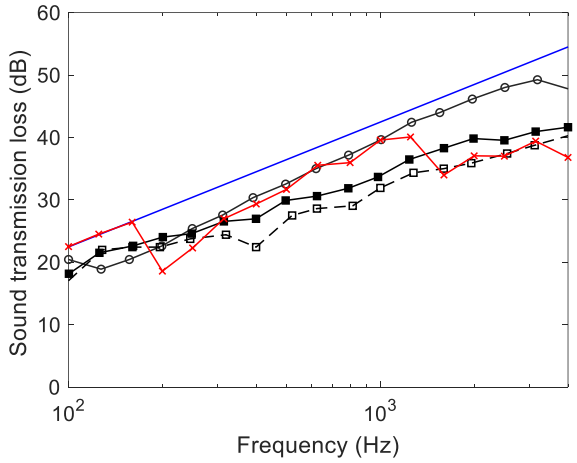

Figure 14. Sound reduction index of the extrusion. —○—: Xie et al.'s SEA model [11], R_w = 36 dB; —×—: the current SEA model, R_w = 34 dB; —■—: measured in [24], R_w = 34 dB; – ▫ –: measured in [42], R_w = 31 dB; —— : mass law for diffuse incidence.

Figure 14 shows that above the first cut-on frequency of the global modes, the sound transmission loss is much smaller than the 'mass law' result. Due to the resonant path, the sound transmission loss of the extruded panel is about 10 dB lower (on average) compared to the non-resonant path (the 'mass law' result), in other words, the transmission coefficient τ of the resonant path will be about 10 times higher than the non-resonant path.

The predicted sound transmission loss from the current SEA model shows there are three dips in the sound transmission loss of this extruded panel. The first one is at about 200 Hz when the first natural frequency of the global modes occurs. Above 1 kHz the modes of all the

subsystems are fully excited, which has caused the second dip at 1.25-1.6 kHz. The critical frequency of the strips occurs at 4.8 kHz and is likely to be the cause of the dip at 4 kHz.

4.2 Sound radiation efficiency

4.2.1 Input power by mechanical excitation

To simulate the radiation efficiency of the extruded panel using the SEA model, a mechanical force is applied to a stiffener or a strip on the bottom plate of the extruded panel (positions indicated in Figure 2). When the force is applied to the stiffener, it is assumed to excite the global vibration directly, whereas when it is applied to the strips it excites both the global and local vibration. The input power is given by

$$P_{\mathrm{in}} = F_{\mathrm{rms}}^2 \,\mathrm{Re}(Y) \tag{25}$$

where F_{rms} is the root mean square force, which is set to unity, and Y is the driving point mobility at the excitation position. It is calculated (for either the response of a strip or the global motion of the whole panel) by using a modal summation assuming simply supported boundaries [14]

$$Y(x_0, y_0) = \frac{4\mathrm{i}\omega}{\mu ab} \sum_{m,n=1}^{\infty} \frac{\sin^2(m\pi x_0/a)\sin^2(n\pi y_0/b)}{\omega_{m,n}^2(1+\mathrm{i}\eta) - \omega^2} \tag{26}$$

where μ is the mass per unit area of the strip / the whole panel, a and b are the corresponding dimensions (equivalent widths are used for the strips). The force location is at (x_0 , y_0), with $0 \le x_0 \le a,\ 0 \le y_0 \le b$, m and n are indices of the modes, η is the damping loss factor and $\omega_{m,n}$ is the $(m,n)^{\mathrm{th}}$ natural frequency. If the force is applied to a stiffener, the driving point mobility is calculated based on modal summation over the global modes. The input power calculated by using Eq. (25) is applied to the global mode subsystem. If the force is acting on a strip, both the global driving point mobility and the local driving point mobility are calculated by using Eq. (26). It is assumed that local modes in other strips do not contribute to the mobility. In this case the input power should be divided between the global mode subsystem and the local mode subsystem on the excitation side according to their mobilities.

Figure 15(a) shows an example of the driving point mobility obtained from Eq. (26) when a force is applied to the stiffener connecting strips B and C (indicated in Figure 2). It is compared with the results obtained from the 2.5D FE model and there is satisfactory agreement between the two results. From inspection of the 2.5D results it has been found that the underestimation at high frequency by the modal summation approach is the result of local motion in the vicinity of the stiffeners caused by their compressional compliance.

Figure 15(b) shows an example of the global and local driving point mobilities when a force is applied on strip B (position indicated in Figure 2). In comparison with the total mobility obtained from the 2.5D FE model, the first natural frequencies of the global and local modes are well predicted. At high frequency, the local driving point mobility is dominant and the calculated result agrees well with the 2.5D FE predicted values. The peak of the local driving point mobility at 1600 Hz is due to the second cut-on mode of the strip in the width direction. Below the first natural frequency of the global modes (186 Hz), the driving point mobility for the local mode subsystem is slightly underestimated by using the modal summation approach, but in this frequency region there are no modes in the extruded panel, thus the subsystems that represent the extruded panel are not included in the SEA model.

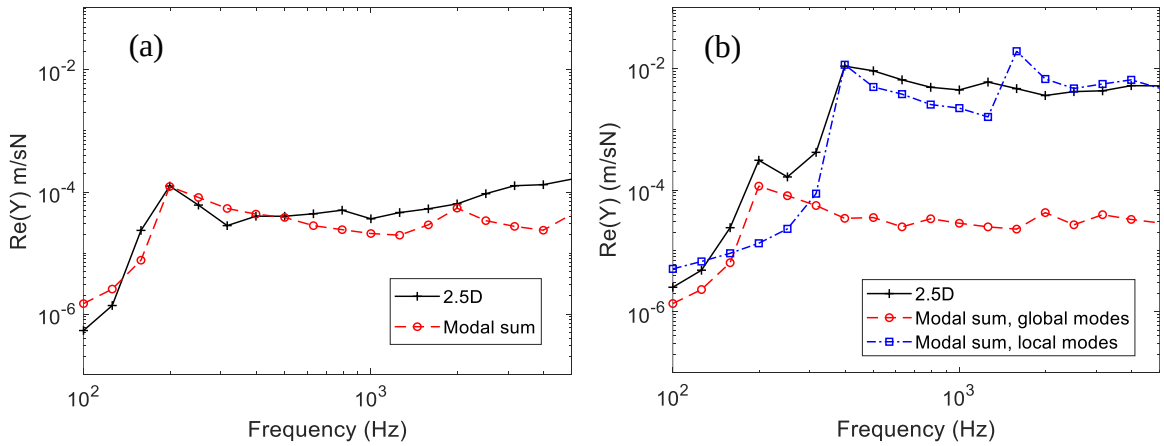

Figure 15. (a) Driving point mobility when a force is applied to the stiffener connecting strip B and C in the mid bay, (b) driving point mobility when a force is applied to strip B. Positions indicated in Figure 2.

4.2.2 Predicted radiation efficiency

The overall radiation efficiency for the panel includes the contributions from the global and local modes. For radiation from one side, it is given by [11]

$$\sigma = \frac{\overline{W}_g + \overline{W}_l}{\rho c S \left\langle \overline{v^2} \right\rangle} = \frac{\rho c S \left\langle \overline{v_g^2} \right\rangle \sigma_g + \rho c S \left\langle \overline{v_l^2} \right\rangle \sigma_l}{\rho c S \left\langle \overline{v_g^2} \right\rangle + \rho c S \left\langle \overline{v_l^2} \right\rangle} = \frac{\left\langle \overline{v_g^2} \right\rangle \sigma_g + \left\langle \overline{v_l^2} \right\rangle \sigma_l}{\left\langle \overline{v_g^2} \right\rangle + \left\langle \overline{v_l^2} \right\rangle} \tag{27}$$

where v_g is the velocity due to global modes, v_l is the velocity due to local modes, σ_g is the radiation efficiency of global modes and σ_l is the radiation efficiency of local modes. S is the area of the extruded panel. $\left\langle \overline{v_g^2} \right\rangle$ and $\left\langle \overline{v_l^2} \right\rangle$ are the time and spatially averaged mean square velocities of the global and local modes obtained from $\left\langle \overline{v_i^2} \right\rangle = E_i/m_i$, where E_i is the energy stored in each subsystem and m_i is the total mass of the subsystem.

There are no available measured results for the radiation efficiency from one side. The sound radiation efficiencies predicted by the SEA model are instead compared with calculations from the 'WANDS' software. Figure 16 shows the results of the extruded panel when the mechanical excitation is applied on strip B in the middle bay and Figure 17 gives the results when excitation is on the stiffener connecting strips B and C.

The SEA model can predict the radiation efficiencies of the extrusion satisfactorily. For excitation on the strip, the SEA model slightly underestimates the results on the excitation side at low frequency. This is partially because the local mobility is overestimated below the first natural frequency, see Figure 15(b). This will increase the contribution of the strips and underestimate the total radiation efficiency of the extrusion at low frequency. On the receiving side, the SEA results agree well with the values obtained from the 2.5D simulations. If the stiffener is excited, see Figure 17, the SEA model can also give good predictions of the radiation efficiency of the extruded panel, especially on the excitation side.

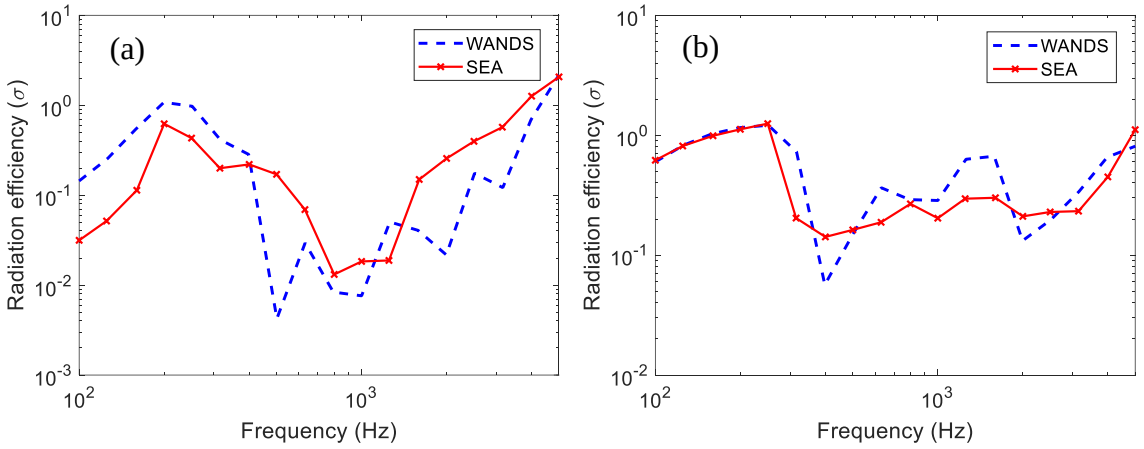

Figure 16. The radiation efficiency predicted by the SEA model compared with results obtained from WANDS software for excitation on strip B, (a) results on excitation side, (b) results on receiving side.

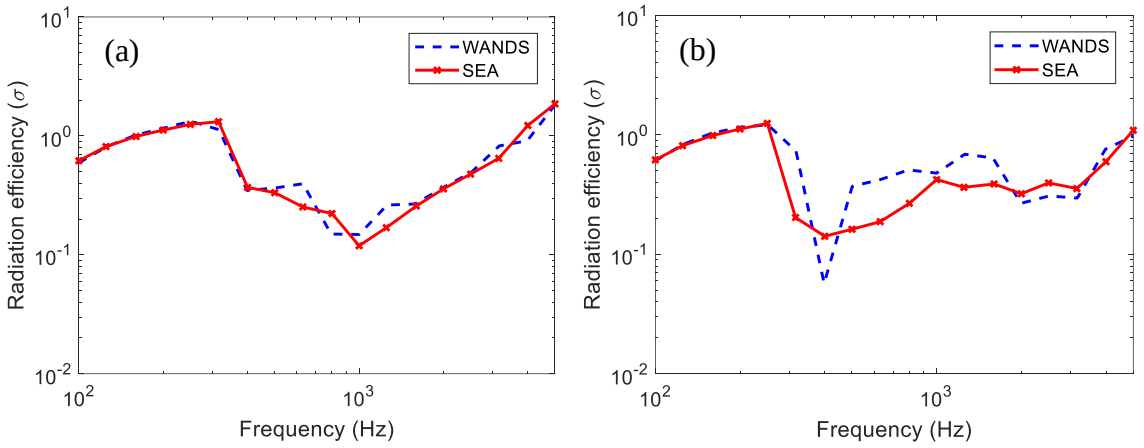

Figure 17. The radiation efficiency predicted by the SEA compared with results obtained from WANDS software for excitation at a stiffener connecting strips B and C, (a) results on excitation side, (b) results on receiving side.

Measurements of the radiation efficiency of this extruded panel can be found in [29, 42], but the measured data includes the radiation from both sides of the panel. In the measurements the extruded panel was suspended by elastic ropes. Two locations on the same strip (P1 and P2) and two at adjacent stiffeners (P3 and P4) were excited. To allow a comparison with these measurements, the measured damping loss factors of the local subsystems are again used in the current SEA model and the results from the two sides of the extrusion are combined. The overall radiation efficiency of the extrusion is calculated by combining the sound power and the averaged mean square velocity of the two sides. The predictions from Xie et al.'s SEA model [11] are also included in the comparisons.

Figure 18(a) shows the comparison of the radiation efficiency when the force is applied at stiffeners P3 and P4. In the measurements some differences appear between the results for these two excitation locations whereas in the SEA model shifting the excitation between P3 and P4 does not make a noticeable difference to the results. From Figure 18(a), it can be seen that Xie et al.'s SEA model and the current one can predict the radiation efficiency with acceptable accuracy above 250 Hz. Below the cut-on frequency of the global modes (186 Hz, indicated in the figure by the dashed line), the two SEA models overestimate the radiation efficiency. This is likely to be because the SEA parameters related to the global modes were determined based on a simply supported extrusion while in the measurements the extrusion is free. The difference in the boundary conditions may have caused the disagreement below the first natural frequency of the extrusion. Figure 18(b) shows the comparison when the excitation is at a strip. P1 and P2 were located on the same strip in the measurements. The SEA model gives similar predictions for excitation at the two locations. Above 1000 Hz, the two SEA models give very similar results. At low frequency, Xie et al.'s model gives a relatively flat prediction while the current model captures the main trend of the radiation efficiency seen in the measurements. The cut-on frequencies of the global and local modes (386 Hz for the local modes) are also indicated in the figure by the dashed lines.

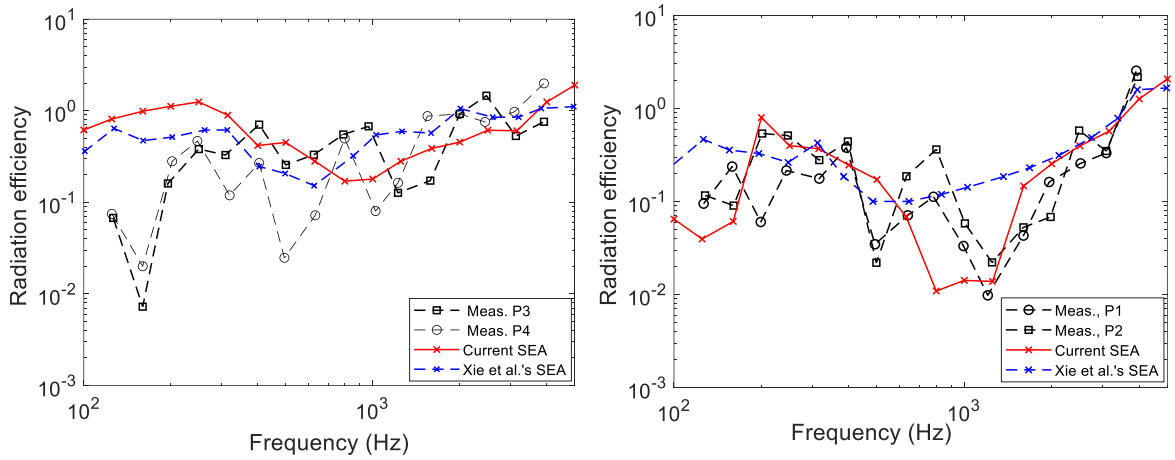

(a) (b)

Figure 18. Prediction of radiation efficiency compared with measurements [29, 42] and Xie et al.'s SEA model [11]. (a) Force on stiffeners, (b) force on strips.

4.3 Comparison with predictions from VA One software

For comparison, the sound transmission loss and the radiation efficiency of this extruded panel have also been determined using the commercial software VA One. This uses a combination of a FE model with periodic structure theory [10] to determine the parameters which are then used in an SEA model. Because the extruded panel is periodic (as shown in Figure 1 there are three periodic cells in the *y* direction) a reduced FE model including one cell of the extruded panel is created in VA One, as shown in Figure 19(a). Its length in the axial direction is set to 1.5 m to correspond to the measured test specimen [29, 42] (it could also be modelled more efficiently by using just a single element in the axial direction). There are about 18,000 elements in the FE model and each element has an approximated size of 10 mm, which allows the calculation up to 5 kHz. In order to be consistent in dimensions with the extruded panel in this work, the FE model is set to repeat twice in the *y* direction. In the length direction, the FE model is set to repeat 13 times, which allows its length to approximate 20 m. The material and damping properties of the extruded panel in the VA One model are taken from Table 2. For comparison with it, the averaged damping loss factors are used in the current analytical SEA model (local subsystems 3 and 4 are assigned a damping factor of 0.005 and local subsystem 5 has a damping loss factor of 0.02 at all frequencies). When using the SEA model to predict the sound transmission loss, the source is added in the acoustic cavity on the lower side in Figure 19(a). In the prediction of the radiation efficiencies, the mechanical force is applied to the structure on the bottom side, as shown in Figure 19(b).

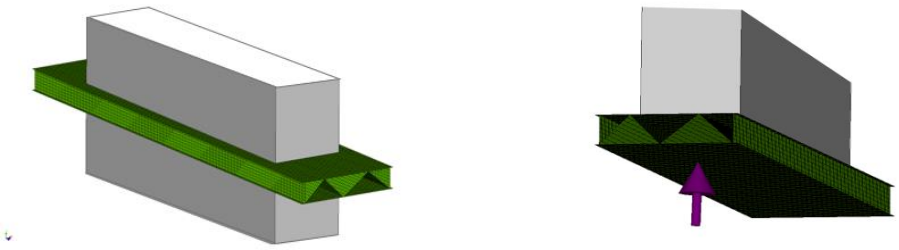

(a) (b)

Figure 19. (a) SEA model in VA One based on the periodic structure theory, (b) the location of the mechanical excitation in the prediction of radiation efficiency.

The sound transmission loss obtained from the SEA model in VA One and the value from the current analytical SEA model in Section 4.1 are compared in Figure 20. They are in reasonable

agreement, although below 315 Hz the current analytical SEA gives better agreement with the measurements.

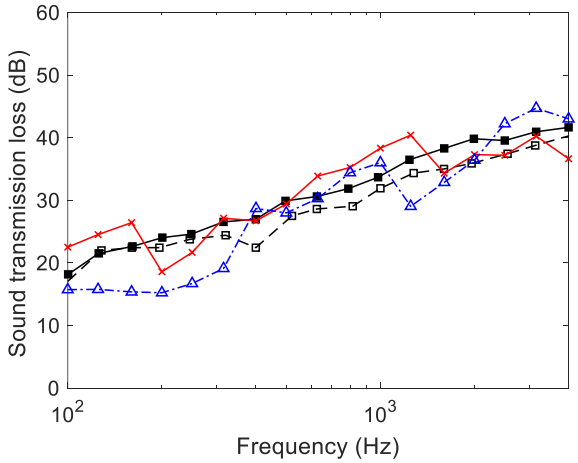

Figure 20. Sound reduction index of the extrusion. —×—: the current SEA model, R_w = 34 dB; -·△·-: VA One software, R_w = 31 dB; —■—: measured in [24], R_w = 34 dB; – ▫ –: measured in [42], R_w = 31 dB.

The radiation efficiencies of the extruded panel obtained from the current analytical SEA model are compared with the predictions from the SEA model in VA One in Figure 21. When the mechanical excitation is applied to the stiffeners, the radiation from the global modes will be dominant at low frequency. The radiation efficiency will drop when the local modes have cut on (at 322 Hz), as shown in Figure 21(a). The results from the current analytical SEA model and the VA One software are of similar accuracy when exciting the stiffeners.

When the mechanical excitation is applied to the strips, the local modes will be dominant in the radiation, leading to lower radiation efficiency even at relatively low frequency, as shown in Figure 21(b). The VA One software presents a slightly better prediction below 1000 Hz while the results from the current analytical SEA model are closer to the measurements above this frequency.

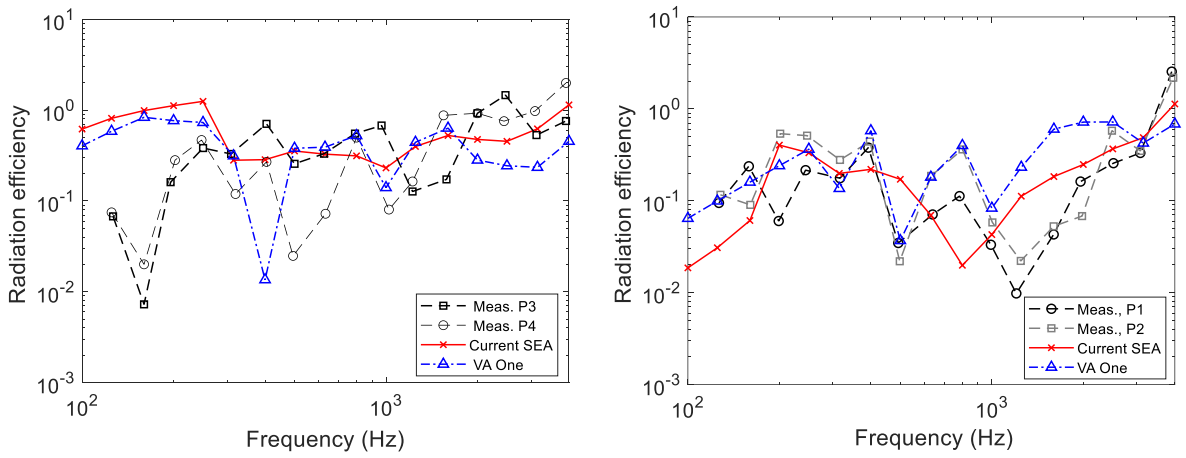

(a) (b)

Figure 21. Prediction of radiation efficiency compared with measurements [29, 42] and VA One software. (a) Force on stiffeners, (b) force on strips.

5 Conclusions

An SEA model is created to study the vibroacoustic behaviour of extruded panels as used in train car bodies, including the radiation efficiency and the sound transmission loss. In the SEA model, the extrusion was separated into four subsystems according to Xie et al. [11], one for global modes and three for local modes. A 2.5D FE model was used to help to determine or validate some essential parameters for the SEA model, in particular, the modal densities of the global and local subsystems, their radiation efficiencies, and the input powers. Each strip could be represented using simply supported boundary conditions if an equivalent width was used, based on the cut-on frequencies obtained from the 2.5D FE model. The average ratio between the original widths and the equivalent ones can be used for extruded panels of different design without the need to implement a 2.5D model. The equivalent widths with simply supported boundary conditions were used in an analytical model to predict the first natural frequency and the modal density of the subsystems, as well as the individual radiation efficiencies of each strip and the input power. The 2.5D FE model is also used as a validation for these parameters. The comparison of these analytically calculated values with the corresponding results from the 2.5D FE model indicates that the equivalent widths of the strips can provide reliable parameters that can be used further for determining the coupling loss factors of the SEA model.

The SEA model can give predictions of sound transmission loss that match measured results with a difference of mostly less than 4 dB. The current approach has shown improvements at high frequency compared with Xie et al.'s SEA model. It was also used to predict the radiation efficiency when a mechanical force is applied either to a stiffener or a strip. For both cases, the SEA model can predict the radiation efficiency on the excitation and receiving sides with good quality and high efficiency compared with the results obtained from the numerical approach (2.5D FE/BE). In comparison with the measured radiation efficiency from the literature, when exciting on the stiffeners, both the current SEA model and Xie et al.'s model can give, on average, acceptable predictions above the cut-on frequency of the global modes. The difference in the boundary conditions between the SEA models and the measurements has possibly caused the disagreement below the cut-on frequency of the global modes. When exciting the strips, the current SEA model captures the main trend of the radiation efficiency and gives satisfactory results compared with the measurements, while Xie et al.'s model gave a relatively flat prediction. The current SEA model is also compared with the VA One software, showing a reasonable agreement.

By following the procedure outlined here, further usage of this SEA model for similar train car body extrusions would not require new numerical models to be developed. Equivalent strips, with a width of 75% that of the ones in the extruded panel and simply supported boundaries, can be used for other similar designs of extrusion and the SEA model can be adopted as a promising predictive approach at an early design stage of railway vehicles.

Acknowledgements

This work is partly funded by the China Scholarship Council.

References

[1]. J. Zhang, X. B. Xiao, X. Z. Sheng, R. Fu, D. Yao, X. S. Jin, Characteristics of interior noise of a Chinese high-speed train under a variety of conditions, Journal of Zhejiang University-SCIENCE A 18(8) (2017) 617-630.

[2]. D. Thompson, Railway noise and vibration: mechanisms, modelling and means of control, Elsevier, 2008.

[3]. D. Thompson, E. Latorre Iglesias, X. Liu, J. Zhu, Recent developments in the prediction and control of aerodynamic noise from high-speed trains, International Journal of Rail Transportation 3(3) (2015) 119-150.

[4]. V. Hongisto, Sound insulation of double panels-comparison of existing prediction models, Acta Acustica United with Acustica 92(1) (2006) 61-78.

[5]. R.H. Lyon, Theory and Application of Statistical Energy Analysis. Elsevier, 2014.

[6]. P. Geissler, D. Neumann, Modelling extruded profiles for railway coaches using SEA. in Proceedings of the 1999 ASME Design engineering technical conferences, September. 1999.

[7]. S Bruhl, P. Faulhaber, M. Grunewald. AutoSEA2 studies on generic light weight structures. in Proc. of the first international AutoSEA users conference, San Diego, CA. 2000.

[8]. U. Orrenius, Y.Y. Pang, B. Stegeman, S. Finnveden, Acoustic modeling of extruded profiles for railway cars, in Novem Saint Raphael, 2005.

[9]. D. Yao, J. Zhang, R.Q. Wang, X.B. Xiao, J.Q. Guo, Lightweight design and sound insulation characteristic optimisation of railway floating floor structures, Applied Acoustics 156 (2019) 66-77.

[10]. V. Cotoni, R. Langley, P. Shorter, A statistical energy analysis subsystem formulation using finite element and periodic structure theory, Journal of Sound and Vibration 318(4-5) (2008) 1077-1108.

[11]. G. Xie, D.J. Thompson, C.J.C. Jones, A modelling approach for the vibroacoustic behaviour of aluminium extrusions used in railway vehicles, Journal of Sound and Vibration 293(3-5) (2006) 921-932.

[12]. G. Xie, D.J. Thompson, C.J.C. Jones, Mode count and modal density of structural systems: relationships with boundary conditions, Journal of Sound and Vibration 274(3-5) (2004) 621-651.

[13]. G. Maidanik, Response of ribbed panels to reverberant acoustic fields, The Journal of the Acoustical Society of America 34(6) (1962) 809-826.

[14]. G. Xie, The vibroacoustic behaviour of aluminium extrusions used in railway vehicles. PhD Thesis, the University of Southampton, 2004.

[15]. S. Finnveden, Evaluation of modal density and group velocity by a finite element method, Journal of Sound and Vibration 273(1-2) (2004) 51-75.

[16]. S. Preis, G. Borello, Prediction of light rail vehicle noise in running condition using SEA. in INTER-NOISE and NOISE-CON Congress and Conference Proceedings. Institute of Noise Control Engineering. 2016.

[17]. D. Manik, A new method for determining coupling loss factors for SEA, Journal of Sound and Vibration 211(3) (1998) 521-526.

[18]. M. Chimeno Manguán, M.J. Fernández de las Heras, E. Roibás Millán, F. Simón Hidalgo, Determination of effective loss factors in reduced SEA models, Journal of Sound and Vibration 386 (2017) 311-326.

[19]. M. Sadri, J. Brunskog, D. Younesian, Application of a Bayesian algorithm for the Statistical Energy model updating of a railway coach, Applied Acoustics 112 (2016) 84-107.

[20]. M.B. Souf, O. Bareille, M.N. Ichchou, B. Troclet, M. Haddar, Variability of coupling loss factors through a wave finite element technique, Journal of Sound and Vibration 332(9) (2013) 2179-2190.

[21]. L. Maxit, J.L. Guyader, Estimation of SEA coupling loss factors using a dual formulation and FEM modal information, part I: theory, Journal of Sound and Vibration 239(5) (2001) 907-930.

[22]. A. Thite, B. Mace, Robust estimation of coupling loss factors from finite element analysis, Journal of Sound and Vibration 303(3-5) (2007) 814-831.

[23]. X. Zheng, Z. Hao, X. Wang, J. Mao, A full-spectrum analysis of high-speed train interior noise under multi-physical-field coupling excitations, Mechanical Systems and Signal Processing 75 (2016) 525-543.

[24]. C.M. Nilsson, A.N. Thite, C.J.C. Jones, D.J. Thompson, Estimation of sound transmission through extruded panels using a coupled waveguide finite element-boundary element method, Notes on Numerical Fluid Mechanics & Multidisciplinary Design 99 (2008) 306-312.

[25]. C.M. Nilsson, C.J.C. Jones, WANDS 2 theory manual, ISVR Technical Memorandum no 975, University of Southampton, 2007. (https://www.southampton.ac.uk/engineering/research/groups/dynamics/rail/wavenumber_finite_and_boundary_elements_with_application_to_railways.page).

[26]. S.K. Datta, A.H. Shah, R.L. Bratton, T. Chakraborty, Wave propagation in laminated composite plates, The Journal of the Acoustical Society of America 83(6) (1988) 2020-2026.

[27]. L. Gavrić, Finite element computation of dispersion properties of thin-walled waveguides, Journal of Sound and Vibration 173(1) (1994) 113-124.

[28]. U. Orrenius, S. Finnveden, Calculation of wave propagation in rib-stiffened plate structures, Journal of Sound and Vibration 198(2) (1996) 203-224.

[29]. H. Kim, J. Ryue, D.J. Thompson, A.D. Müller, Prediction of radiation ratio and sound transmission of complex extruded panel using wavenumber domain finite element and boundary element methods. MOVIC2016 & RASD2016, Journal of Physics: Conference Series, 744 (2016) 012144.

[30]. H. Kim, J. Ryue, D.J. Thompson, A.D. Müller, Application of a wavenumber domain numerical method to the prediction of the radiation efficiency and sound transmission of complex extruded panels, Journal of Sound and Vibration 449 (2019) 98-120.

[31]. Y. Zhang, D. Thompson, G. Squicciarini, J. Ryue, X. Xiao, Z. Wen, Sound transmission loss properties of truss core extruded panels, Applied Acoustics 131 (2018) 134-153.

[32]. T. Kohrs, B.A. Petersson, Wave beaming and wave propagation in light weight plates with truss-like cores, Journal of Sound and Vibration 321(1-2) (2009) 137-165.

[33]. Y. Yang, B.R. Mace, M.J. Kingan, A wave and finite element based homogenised model for predicting sound transmission through honeycomb panels, Journal of Sound and Vibration 463 (2019) 114963.

[34]. U. Orrenius, H. Liu, A. Wareing, S. Finnveden, V. Cotoni, Wave modelling in predictive vibro-acoustics: Applications to rail vehicles and aircraft, Wave Motion 51(4) (2014) 635-649.

[35]. A.W. Leissa, Vibration of plates. Ohio State Univ Columbus, 1969.

[36]. D.J. Thompson, N.S. Ferguson, J.W. Yoo, J. Rohlfing, Structural waveguide behaviour of a beam–plate system, Journal of Sound and Vibration 318(1-2) (2008) 206-226.

[37]. R.J.M. Craik, Sound transmission through buildings : using statistical energy analysis. Aldershot: England Gower Publishing Limited. 1996.

[38]. F. Fahy, D. Thompson, Fundamentals of sound and vibration, second edition, CRC Press, 2016.

[39]. G. Xie, D. Thompson, C. Jones, The radiation efficiency of baffled plates and strips, Journal of Sound and Vibration 280(1-2) (2005) 181-209.

[40]. M. Heckl, Wave Propagation on Beam-Plate Systems, The Journal of the Acoustical Society of America 33(5) (1961) 640-651.

[41]. G.L. Lamb, Input Impedance of a Beam Coupled to a Plate, The Journal of the Acoustical Society of America 33(5) (1961) 628-633.

[42]. A.D. Müller, Acoustical investigation of an extruded aluminium railway vehicle floor panel. MSc Thesis, University of Southampton, 2004.

[43]. ISO 717–1:2013. Acoustics – Rating of sound insulation in buildings and of building elements – Part 1: Airborne sound insulation.